Divergent Responses of Summer Precipitation in China to 1.5°C Global Warming in Transient and Stabilized Scenarios

Zhihong Jiang, Qiyao Hou, Tim Li, Yongxiao Liang, Laurent Li

Divergent Responses of Summer Precipitation in China to 1.5°C Global Warming in Transient and Stabilized Scenarios

Zhihong Jiang[1,2]*, Qiyao Hou[1], Tim Li[2,3], Yongxiao Liang[1,4], Laurent Li[5]

[1]*Joint International Research Laboratory of Climate and Environment Change, Collaborative Innovation Center on Forecast and Evaluation of Meteorological Disaster, Nanjing University of Information Science and Technology, Nanjing* 210044, *China*.

[2]*Key Laboratory of Meteorological Disaster of Ministry of Education, Collaborative Innovation Center on Forecast and Evaluation of Meteorological Disaster, Nanjing University of Information Science and Technology, Nanjing* 210044, *China*.

[3]*International Pacific Research Center (IPRC), and Department of Atmospheric Sciences, SOEST, University of Hawaii at Manoa, Honolulu, HI 96822, USA.*

[4]*School of Earth and Ocean Sciences, University of Victoria, Victoria, British Columbia, Canada*.

[5]*Laboratoire de Météorologie Dynamique, IPSL, CNRS, Sorbonne Université, Ecole Normale Supérieure, Ecole Polytechnique, Paris* 75005, *France*.

Corresponding author: Zhihong Jiang (zhjiang@nuist.edu.cn)

Key Points:

- The summer precipitation increases more significantly in southeast China in the stabilized warming scenario compared with the transient one
- The dynamic effect in relation to changes of atmospheric circulation constitutes the major discriminant factor of distinctive precipitation responses
- The differential meridional thermal gradient related to a contrasted land-ocean warming leads to dynamic changes

Abstract

Responses of summer precipitation in China to global 1.5°C warming with transient and stabilized pathways are investigated through the analysis of the Common Earth System Model climate simulations. Precipitation increases more significantly in southeast China in the stabilized scenario compared with the transient one. The difference is primarily attributable to dynamic factors related to circulation changes and driven by differences of land–ocean thermal contrast between the two scenarios. The stabilized warming favors conditions of larger ocean warming and smaller land warming, leads to enhanced meridional temperature gradient and ultimately speeds up the jet stream over East Asia. Ageostrophic wind at the entrance of the accelerated jet strengthens ascending motion and precipitation along the coast of Asia from southeast China to India. The enhanced heating over India further induces a Kelvin-wave response with an anomalous anticyclone that contributes to the enhanced westward shifted of the western North Pacific Subtropical High. Southerly winds at the west flank of the anticyclone transport moisture northward from tropical oceans, and strengthen precipitation in southeast China.

Plain Language Summary

This study deals with the issue of regional precipitation response to 1.5°C global warming in accordance to the Paris Agreement on Climate Change for two different pathways, either transient or stabilized. Compared with the transient warming scenario, summer precipitation increases more significantly in southeast China in the stabilized one. This feature of distinctive precipitation responses, with strong implications for policy making in terms of regional climate mitigation and adaptation, is furthermore explored through a moisture budget analysis. Dynamic effect in relation to changes of atmospheric circulation is found to be the major contributor to the difference. The cause of the significant difference in precipitation in South China is attributed to changes of land-ocean thermal contrast, leading to a series of atmospheric circulation adjustments. Results presented here satisfactorily addressed, for the first time, the long-standing issue on global warming, namely, how the atmosphere responds distinctively under the transient and stabilized anthropogenic forcing pathways which show however an identical global warming level.

1. Introduction

The Paris Agreement adopted at the UNFCCC 21st conference of parties in 2015 aims to limit global warming to less than 2°C and to pursue efforts to limit the global warming level to 1.5°C (UNFCCC, 2015). The Agreement nevertheless did not mention any pathways to reach the goal. There are actually different scenarios to achieve the 1.5/2°C warming target. At least two possibilities are offered to us, with either a transient warming scenario or a stabilized one (Zhai et al., 2017). Although the two pathways can reach to an identical global warming level, climate change may be divergent at regional scale (Boulange et al., 2018; King et al., 2019).

The Coupled Model Inter-comparison Project Phase 5 (CMIP5), with its coordinated ensemble simulations from multiple models and multiple emission paths (including RCP2.6, RCP4.5 and RCP8.5), is the most important effort of the international scientific community in dealing with climate change. But it is of transient conditions, as the global warming levels, 1.5°C and 2°C, are gradually reached and then exceeded (King et al., 2019; Zhang & Villarini, 2017; Chevuturi et al., 2018; Lee et al., 2018; Li et al., 2018). Such an approach does not seem entirely satisfy the spirit of the Paris Agreement which tends to refer to stabilized climate (Rogelj et al., 2019; Wehner et al., 2017; Wei et al., 2019). Recently, the Community Earth System Model (CESM) low-warming simulations performed by the National Center for Atmospheric Research (NCAR) provides an opportunity for assessing climate changes at stabilized levels (Sanderson et al., 2017). It is worth investigating what are the divergent responses between transient and stabilized warming scenarios and why they occur.

East China has a very prominent monsoonal climate with dry and cold winter, but humid and hot summer. The East Asian summer monsoon plays thus an important role in the regional climate variability. But its future evolution within the global warming context is of high uncertainty, since the consensus among CMIP models is low with divergent results. Before going further, we can summarize a few main works for the East Asian summer monsoon, as synthetized in the IPCC special report on the impacts of global warming of 1.5°C (IPCC, 2018). Most studies are based on transient scenarios from CMIP5 models. Both total precipitation and extreme precipitation would increase over East Asia under RCP scenarios (Kitoh et al., 2013; Li et al., 2015; Alfieri et al., 2016). The precipitation seasonal cycle would be enhanced, and a lower warming target could robustly reduce hydrological risks compared to higher warming levels (Zhang et al., 2019). Further research shows that the risk of flooding would be increasing significantly in many areas of China, especially in western China and the Huanghuai Basin (Li et al., 2018). The summer monsoon intensity would experience a significant increase causing an enhancement of precipitation in north of East Asia under the 1.5°C warming scenario (Liu et al., 2018).

There are also a few recent studies reported in the literature (Lee et al., 2018; Chen et al., 2018; Li et al., 2019; Chen et al., 2020) to assess changes of the East Asian

summer monsoon system in the stabilized 1.5°C and 2°C warmer worlds. Although results from the stabilized and transient scenarios are qualitatively consistent in projecting an increased frequency and intensity of extreme precipitation over East Asia, there exist significant differences in the response of summer monsoon and in the spatial structures of precipitation. In this article, we would like to revisit this issue of transient/equilibrium pathways, with emphasize on the underlying dynamic-physical mechanisms. In particular, what are the thermodynamic effects in relation to water vapor changes? and what are the dynamic effects in relation to regional atmospheric circulation?

In this study, the CESM large ensemble simulations including RCP8.5 and low-warming scenarios were used to analyze the changes in summer precipitation over China under stabilized and transient 1.5°C warming scenarios, with a focus on the difference between the two scenarios. We also analyze the outputs from CMIP5 multi-model ensemble (CMIP5_MME, see Supplementary materials, Table S1) and compare results with the CESM large ensemble simulations to assess the robustness of our findings.

2. Data and Methods

2.1 Data source

Main data used in this study originate in the Community Earth System Model (CESM), developed and operated by the National Center for Atmospheric Research (NCAR). CESM has been largely used in studies on the East Asian Summer Monsoon. It shows very good performance in simulating the regional precipitation and monsoon circulation (Kay et al., 2015). From the ESGF platform, we downloaded relevant simulations from the experiments CESM_LENS (large ensemble) and CESM_LW (low warming stabilized at 1.5°C) (Sanderson et al., 2017). We obtained 11 members from the ensemble and for both experiments. Daily precipitation and monthly circulation outputs of the historical simulation (1850-2005) and future projections (2006-2100, under the scenario RCP8.5) were downloaded for our purpose. The synergy combining the CESM large ensemble runs and the CESM low-warming runs provides an ideal framework to investigate the differences between transient and stabilized scenarios. Greenhouse gas (GHG) emission pathways and aerosol forcing both differ among the two different scenarios (Sanderson et al., 2017; Zhang and Zhou, 2021), other aspects of CESM being identical. Both experiments contain 11 ensemble members with different initial conditions. Climate internal variability may play a dominant role on regional climate change, particularly for rainfall (Deser et al., 2012). The ensemble approach helps remove internal climate variability and obtain robust signal of forced climate change (Lo & Hsu, 2010; Guan et al., 2015; Huang et al., 2017). In addition, the CMIP5 multi-model ensemble, as an equivalent of our transient scenario is also used to assess the robustness of our work. Actually, we downloaded data of 21 coupled global climate models from the CMIP5 RCP8.5 scenario experiment (Table S1).

2.2 Timing of the 1.5°C warming target

As a general practice, changes of any climate variables or indices are evaluated with reference to present day defined as the period of 1986-2005, although the timing of the 1.5°C warming target is relative to preindustrial. For the transient scenario from CESM_LENS, the global and annual mean surface air temperature was firstly processed to form a long time series from 1850 to 2005, and then from 2006 to 2100 following the RCP85 scenario. As used in Shi et al., (2018), the time series of each individual member was smoothed with a 20-year running-mean filter. We can then detect the year when the warming target (1.5°C relative to pre-industrial) is reached, which determines our working window of 20 years. For the 11 members of CESM_LENS, we actually obtained years 2020-2039 as the window of 1.5°C global warming. For the CMIP5_MME, the time periods of 1.5°C global warming for each individual model were also selected in the same way as for CESM_LENS. It is worth noting that the actual global warming when the 1.5°C threshold is reached is only 0.9°C with reference to present-day climate from 1986 to 2005.

For the stabilized warming scenario, CESM_LW, since its design was to keep a stabilized warming level of 1.5°C for the whole duration, we decided to use the end of the simulation as our investigation time window to have a better stabilized state. This corresponds, nominatively, to the last 20 years (2081-2100) of the 21st century (in agreement with most other similar studies, such as Wei et al., 2019 and Li et al., 2019).

2.3 Moist budget analysis

For vertically-integrated water vapor, we can easily establish its budget equation as:

$$\partial_t \langle q \rangle + \langle \overrightarrow{V_h} \nabla_h q \rangle + \langle \omega \partial_p q \rangle = E - P \quad (1)$$

where P is precipitation rate, E evaporation rate at surface. q represents the specific humidity. V_h represents the horizonal wind while ω is the vertical velocity at pressure level. $<>$ represents the column integration for the whole layer from 1000 to 100 hPa. ∂_t and ∂_p denote time and pressure derivatives respectively. The time derivative term $\partial_t < q >$ is generally small and can be ignored for long term mean. If we assume that climate change is a perturbation added to the basic climatology, the moisture budget equation can be transformed into its derivative form or perturbation form:

$$P' = E' - \langle \overrightarrow{V_h} \nabla_h q \rangle' - \langle \omega \partial_p q \rangle' \quad (2)$$

$\langle -\overrightarrow{V_h} \nabla_h q \rangle'$ represents the anomaly of water vapor horizontal advection, and it is generally smaller than the vertical advection term $\langle -\omega \partial_p q \rangle'$. The vertical advection term, as a first order approximation, can be decomposed into two combined linear

effects, one related to changes of specific humidity (called as thermodynamic contribution, TC) and another related to changes of circulation (called as dynamic contribution, DC) (Chou & Lan, 2012):

$$\langle -\omega \partial_p q \rangle' = \langle -\bar{\omega} \partial_p q' \rangle + \langle -\omega' \partial_p \bar{q} \rangle + Res \quad (3)$$

The bar ($\bar{}$) denotes the historical climatological monthly mean, and the prime ($'$) represents the departure from the mean. The term $\langle -\bar{\omega} \partial_p q' \rangle$ is the advection of anomalous water vapor by climatological vertical wind (also called thermodynamic effect), and the term $\langle -\omega' \partial_p \bar{q} \rangle$ is the advection of climatological water vapor by anomalous vertical wind (also called dynamic effect). The residual term includes also the non-linear contribution. This methodology is a commonly-used moisture budget analysis for a diversity of applications to investigate regional precipitation changes for different warming scenarios (Chou & Lan, 2012; Chou et al., 2013).

This decomposition permits us to explore the relative contribution of changes in water vapor and in atmospheric circulation to the change of precipitation. The thermodynamic term $-< \bar{\omega} \partial_p q' >$ is directly determined by the change in air humidity. According to the Clausius-Clapeyron equation, the change of this term is closely related to the change of temperature. While the dynamic term $-< \omega' \partial_p \bar{q} >$ is closely related to the change of large-scale vertical motion. Each component in Eq. (3) is calculated using the monthly data of the CESM ensemble members, and then the multimember mean is calculated.

3. Results

3.1 Different responses of summer (JJA) precipitation

The structural change of JJA precipitation under stabilized and transient warming scenarios in the 1.5°C warmer climate is examined first and shown in Figure 1a-c. Precipitation increases in most areas of China under the stabilized scenario, with hotspots being seen in southeast China and northwest China (Figure 1a). The increase is by more than 10% in most parts of southeast China. For the transient warming scenario, precipitation increases by more than 6% in most parts of northwest and northeast China, but there is no significant increase in southeast China. It is clear that southeast China (22-33°N, 105-122°E, land areas) is the region with the largest difference between the transient and stabilized warming scenarios. It is worthy of note that results from CESM_LENS are quite comparable to its counterpart from CMIP5_MME, as demonstrated in Figure 1c showing the multi-model ensemble mean results of available CMIP5 models. Conclusions that we can draw from the current work might be robust among different CMIP5 models.

This is further confirmed by the regional mean calculated for whole China and southeast China, respectively. Results are shown in Figure 1d. The regional-mean

change for whole China increases by approximately 12.1% in CESM_LW, while by only 7.4% and 5.2% in CESM_LENS and CMIP5_MME. In southeast China, the regional mean changes in total precipitation increases by approximately 19.3% in CESM_LW, while only 6% and 3.7% in CESM_LENS and CMIP5_MME. We also evaluate the uncertainty manifested as the ensemble range, and shown by bars in Fig. 1d. We can see that the changes of JJA precipitation in southeast China are quite different between the two scenarios, with a more significant increase in the stabilized warming scenario.

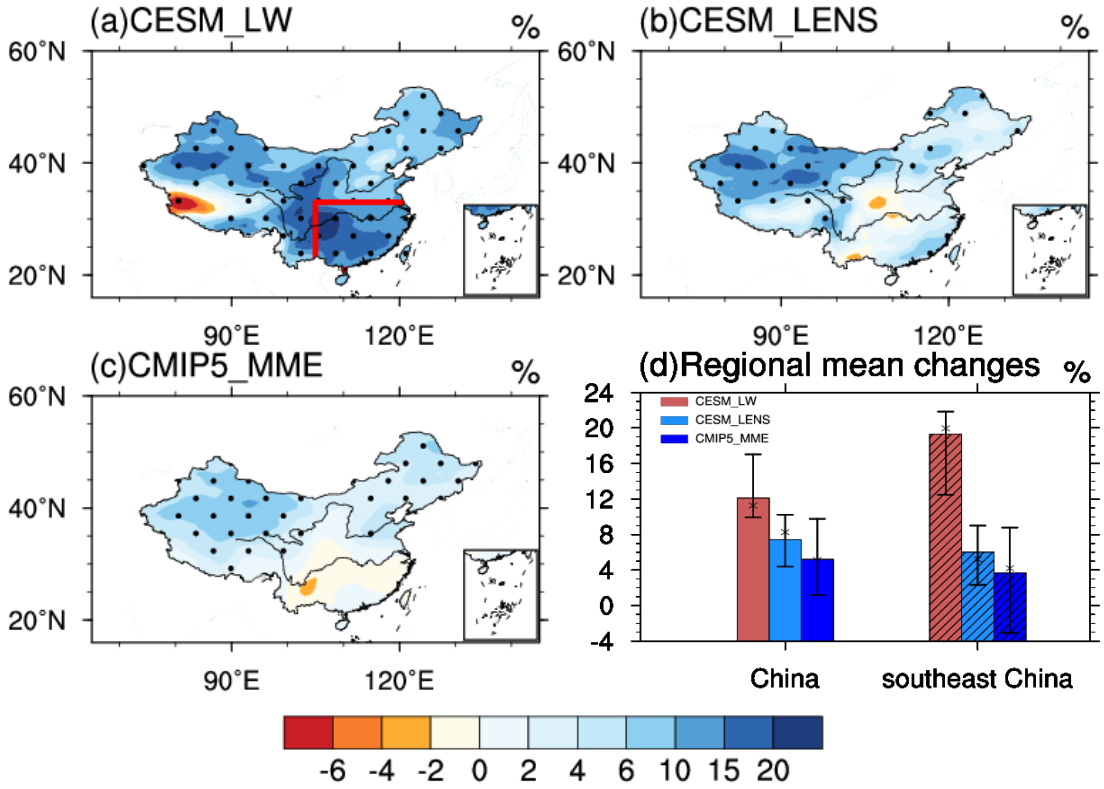

Figure 1. Transient scenario and stabilized scenario reveal significant differences of precipitation responses to 1.5°C global warming for whole China and especially for Southeast China. Panels **a**, **b** and **c** displays the relative changes of summer (JJA) precipitation (relative to 1986-2005, considered as present-day climate) in the 1.5°C warmer climate (relative to preindustrial), obtained with CESM low-warming simulations (noted as CESM_LW, stabilized warming scenario, panel **a**), with CESM large-ensemble simulations (noted as CESM_LENS, transient warming scenario, panel **b**), and with all available CMIP5 models in their ensemble-mean form (noted as CMIP5_MME, transient warming scenario, panel **c**). The red box indicates southeast China, our target domain (22-33°N, 105-122°E, land areas). Panel **d** is the areal mean over the red box. Error bars denote the range of the ensemble members, and the symbols represent the median of the ensemble. The dotted areas in **a-c** are statistically significant at the 5% level for the differences between the stabilized and transient scenarios.

We also observed similar behaviors for some extreme precipitation indices, such as the maximum precipitation for five consecutive days (Rx5day, shown in Figure S1),

which are useful and relevant for societal vulnerability assessment. Compared to Zhang and Zhou (2019) using CMIP5 multi-model projections, the change of Rx5day is here more pronounced in southeast China, indicating an enhanced effect under the stabilized scenario.

Therefore, it is of great significance to further explore mechanisms that contribute to the projected differences between the two warming scenarios, particularly for changes in southeast China.

3.2 Moisture budget analysis

To further understand physical processes leading to the precipitation changes, an analysis of the vertically-integrated moisture budget (as described in Methods, Eq. 2) was performed. The two advection terms are linearly decomposed into dynamic effects (in relation to atmospheric circulation) and thermodynamic effects (in relation to water vapor changes). Since the horizontal advection term is generally small, we will limit our analysis of dynamic and thermodynamic effects to the only effects from the vertical advection, as shown in Figure 2 (regional maps) for the two warming scenarios respectively.

It can be seen that, for the stabilized warming scenario, both dynamic and thermodynamic terms contribute to precipitation enhancement in southeast China, and the dynamic contribution is significantly larger than the thermodynamic contribution. This is particularly true for the middle and lower reaches of the Yangtze River. It is worth noting that strong values of the dynamic contribution are located in the south edge of the Tibetan Plateau and in southeast China, actual regions of much enhanced precipitation under the stabilized scenario. In northern China and northeastern China, the dynamic contribution shows negative values, while the thermodynamic contribution is insignificantly positive, which partially explains the less important increase of precipitation in these regions. For the transient warming scenario, it is clear that the thermodynamic contribution, as in the stabilized scenario, enhances precipitation in most regions of China, especially in the east and south of the Tibetan Plateau. However, the dynamic contribution shows much smaller values, compared to the stabilized scenario. This is particularly true in southeast China and in the Yangtze River Basin where even negative values are found.

Figure 2e shows the regional average of each term of the moisture budget equation, with the vertical advection term decomposed into dynamic and thermodynamic contributions, in southeast China (22-33°N, 105-122°E). As expected, the horizontal advection term $-\langle\overrightarrow{V_h}\nabla_h q\rangle'$ is much smaller than the vertical advection term. For the stabilized warming (transient warming) scenario, the contribution of dynamic term is about 0.64 (0.33) mm/day, while that of thermodynamic term is about 0.28 (0.22) mm/day in southeast China. Again, we can see that, the dynamic contribution in the two scenarios is quite different. The dynamic contribution in the stabilized scenario is about

twice larger than its counterpart in the transient scenario. Therefore, the difference of precipitation changes, between the transient and stabilized scenarios, for the same warming threshold of 1.5°C, is mainly caused by the difference in dynamic terms in southeast China. Finally, we need to point out that, in both the transient and stabilized scenarios, the evaporation in southeast China increases and contributes positively to the enhancement of precipitation. This is a manifestation of intensification of the local water recycling in response to global warming.

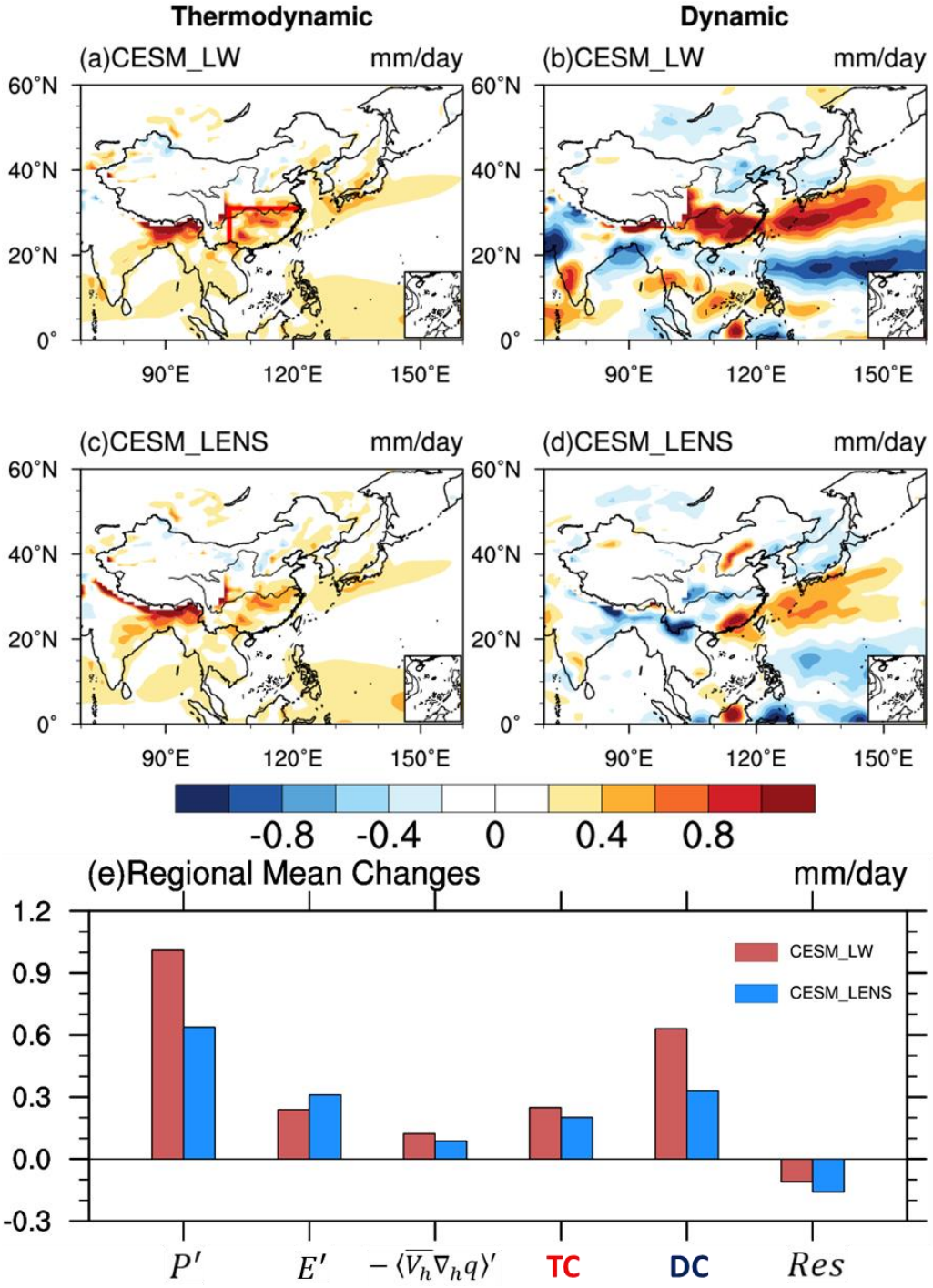

Figure 2. Decomposition of the moisture budget equation allows to quantitatively measure different contributing terms to the total precipitation response, and in particular, to evaluate the thermodynamic contribution (TC) and dynamic contribution (DC). The dynamic effect constitutes the major differentiating factor between the two scenarios. Panels **a** to **d** displays the thermodynamic, dynamic effects in the two scenarios CESM_LW and CESM-LENS for the same 1.5°C global warmer climate. Panel **e** displays the regional area-averaged moisture budget components (mm/day) for southeast China.

The positive contribution of the dynamic term under the stabilized warming scenario indicates that the projected future atmospheric circulation behaves in such a way that precipitation increases. Since the analyses above are the results of vertical integration, we need to further investigate the vertical distribution of changes for vertical velocity ω and water vapor q over southeast China (Supplementary Figure 1). For the vertical velocity $-\omega'$, compared to CESM_LENS, there are large values in the whole layer in CESM_LW, with a maximum of about 0.5×10^{-2} Pa/s located at 300hPa. There is consequently a strong ascending motion in this area, which is conducive to the increase of precipitation. However, changes in specific humidity q are almost the same in the two scenarios. The change in specific humidity q in CESM_LW is larger in the lower atmosphere at 1000-850hPa, while that in CESM_LENS is larger in the middle and upper atmosphere. Such vertical distribution characteristics are consistent with the analysis of the vertically-integrated moisture budget and confirm that the changes in vertical velocity of the whole layer (dynamic effect) constitute the main contributor to the enhancement of precipitation, while the difference in specific humidity (thermodynamic effect) is quite small between the two warming scenarios.

3.3 Atmospheric thermal structure

The analysis of the water vapor balance equation clearly indicates that the dynamic term in the vertical advection of water vapor is the key to explain the divergent response of precipitation between the two warming scenarios in southeast China. We need to explore how and why the regional atmospheric circulation behaves differently. Our intuition conducted us to firstly examine the regional land-sea thermal contrast which is the primary driver for the East Asian summer monsoon (EASM) and precipitation in Southeast China (Wang et al., 2000). Figure 3 shows the spatial distribution of surface temperature for the two warming scenarios (noted as Δ) and their difference (noted as δ). It can be seen that most land areas show temperature increase by more than 1.5°C in the transient scenario, while the increase is generally less than 1°C in the stabilized scenario. The latter shows, however, a much warmer zone over oceans and along the Asian coasts with temperature increase exceeding 1°C. These characteristics can be more clearly seen in the differential map in Figure 3c showing the second-order difference (noted as δΔ). Most land areas of Eurasia and North America (especially, north of 30°N) are cooler by 0.5°C in the stabilized scenario, while most maritime areas of the Indian and Pacific Oceans, as well as the Indian Peninsula and the Asian coasts (south of 30°N) are 0.5°C warmer. Such a contrast between ocean and land is consistent with previous studies showing the warming response is much slower over ocean than

over land (Long et al., 2014). With a global warming level stabilized at 1.5°C, the stabilized scenario inevitably shows smaller warming over lands and larger warming over oceans.

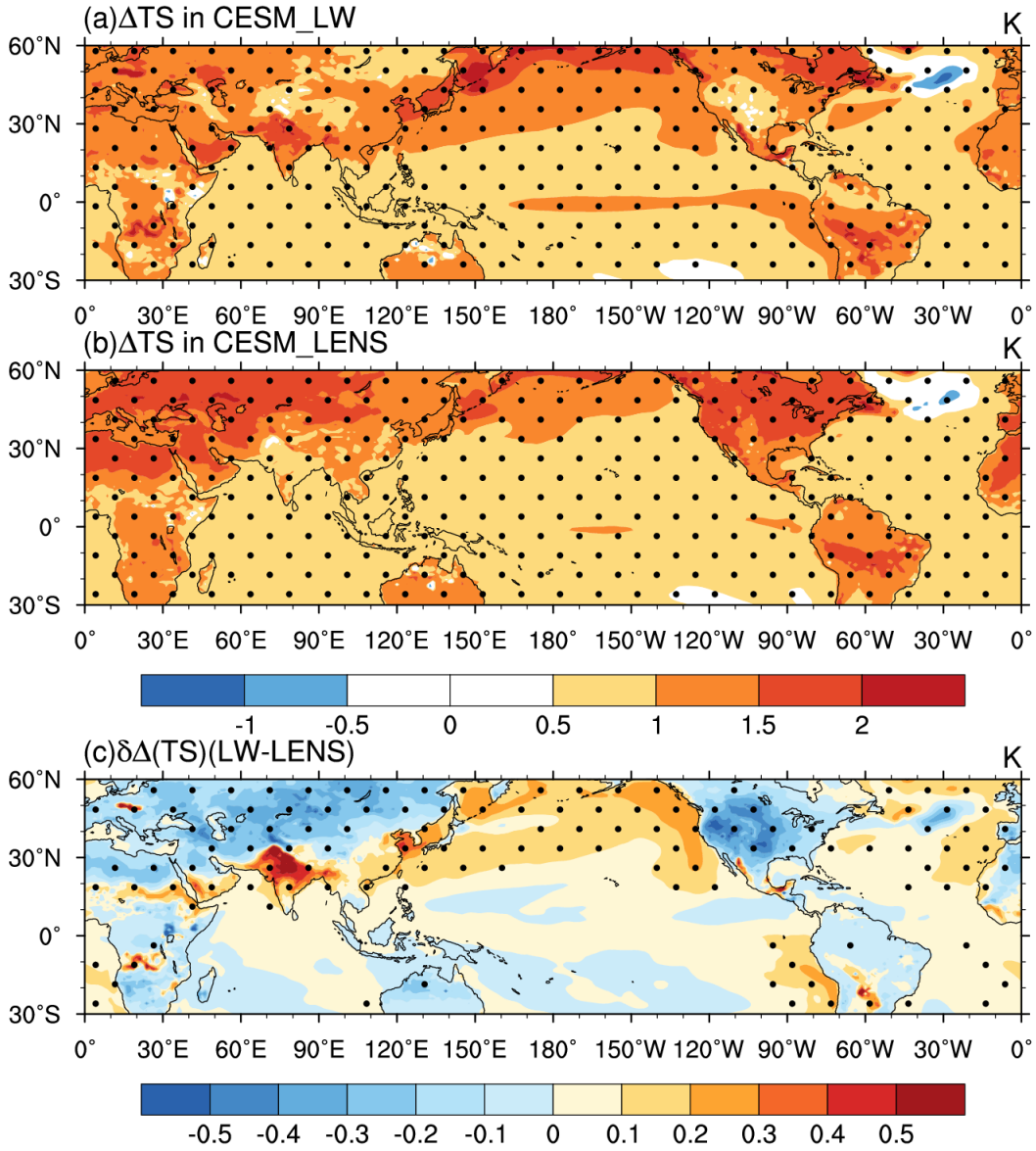

Figure 3. The two scenarios (transient CESM_LENS and stabilized CESM_LW) reveal different structural changes of surface temperature ΔTS for the same 1.5°C warmer global climate, with colder land and warmer ocean in the stabilized scenario. **a**, The spatial distribution of ΔTS under the stabilized warming scenario. **b**, Same as **a** but for the transient warming scenario. **c**, The difference δ(ΔTS) between the stabilized and transient warming scenarios. The dotted areas in **a** and **b** are statistically significant at the 5% level for the differences between 1.5°C warmer climate and present-day climate, in **c** are statistically significant at the 5% level for the differences between the stabilized and transient scenarios.

Beyond the differential warming rates between land and ocean under stabilized and transient scenarios, another factor contributing to the difference of atmospheric

thermal structure is the emission projection of aerosols, differently implemented in the two CESM simulations (Fig. 4, showing relative changes of JJA aerosol optical depth), with consequences on both mean and extreme temperatures expected over major aerosol source regions, such as India and South and East China (Wang et al., 2017; Li et al., 2015). Actually, there is an obvious decrease of aerosol loading in South and East China land areas in CESM_LW, while aerosols continue to increase over India and over the Asian monsoon areas in CESM_LENS when the 1.5°C global warming threshold is reached. It is clear that the difference of aerosol forcing over the Indian Peninsula and land areas of South and East Asia can partly explain the relative warming structure over India and East Asia (as in Figure 3c). Our results on both surface air temperature and precipitation corroborate what shown by Li et al. (2015) and Zhou et al. (2020).

In the configuration that the surface temperature dominates and plays an active role, its increase leads to lower sea-level pressure and unstable stratification, which favors low-level convergence, ascending motion and occurrence of rainfall. It is however worthy of note that the relationship between surface air temperature and precipitation can be complex under global warming, especially at regional scale. Actually, positive rainfall change may lead to negative surface temperature change through increased cloudiness and surface evaporation (Mueller and Seneviratne, 2020). In our case of CO_2 forcing scenario, the surface air temperature responds quickly to the land surface warming at the Eurasian continental scale, and provokes changes of large-scale atmospheric circulation.

We further investigate how the atmosphere circulation changes between stabilized and transient scenarios. The distinct changes in land and sea surface temperature leads to larger meridional temperature gradient and vertical wind shear over 30-40°N. Figure 5a displays the second-order variation (noted as $\delta\Delta$, with Δ indicating the 1.5°C global warming and δ the difference between CESM_LW and CESM_LENS) for atmospheric temperature T (integrated from 850 to 200 hPa) and its meridional gradient $-\partial T/\partial Y$. It can be seen that there is a larger temperature gradient change under the stabilized warming scenario, while the whole layer temperature is more than 0.2°C warmer in the south of 30°N and 0.1°C cooler in the north of 40°N. Compared to the transient warming scenario, the temperature meridional gradient $-\partial T/\partial Y$ is approximately 0.04K/100km larger near 30°N under the stabilized warming scenario. With the thermal wind relationship, a stronger vertical shear of zonal wind is generated. Figure 5b displays the changes of zonal wind u at 200hPa, superimposed with the CESM model climatological u. In the upper atmosphere at 200hPa, the differential zonal wind westerly jet is centered at 30-40°N with the main body (2 m/s) extending from East China to Japan, and to the North Pacific. There is a clear southeastward shift and intensification for the climatological zonal wind westerly jet which is centered at 35-45°N.

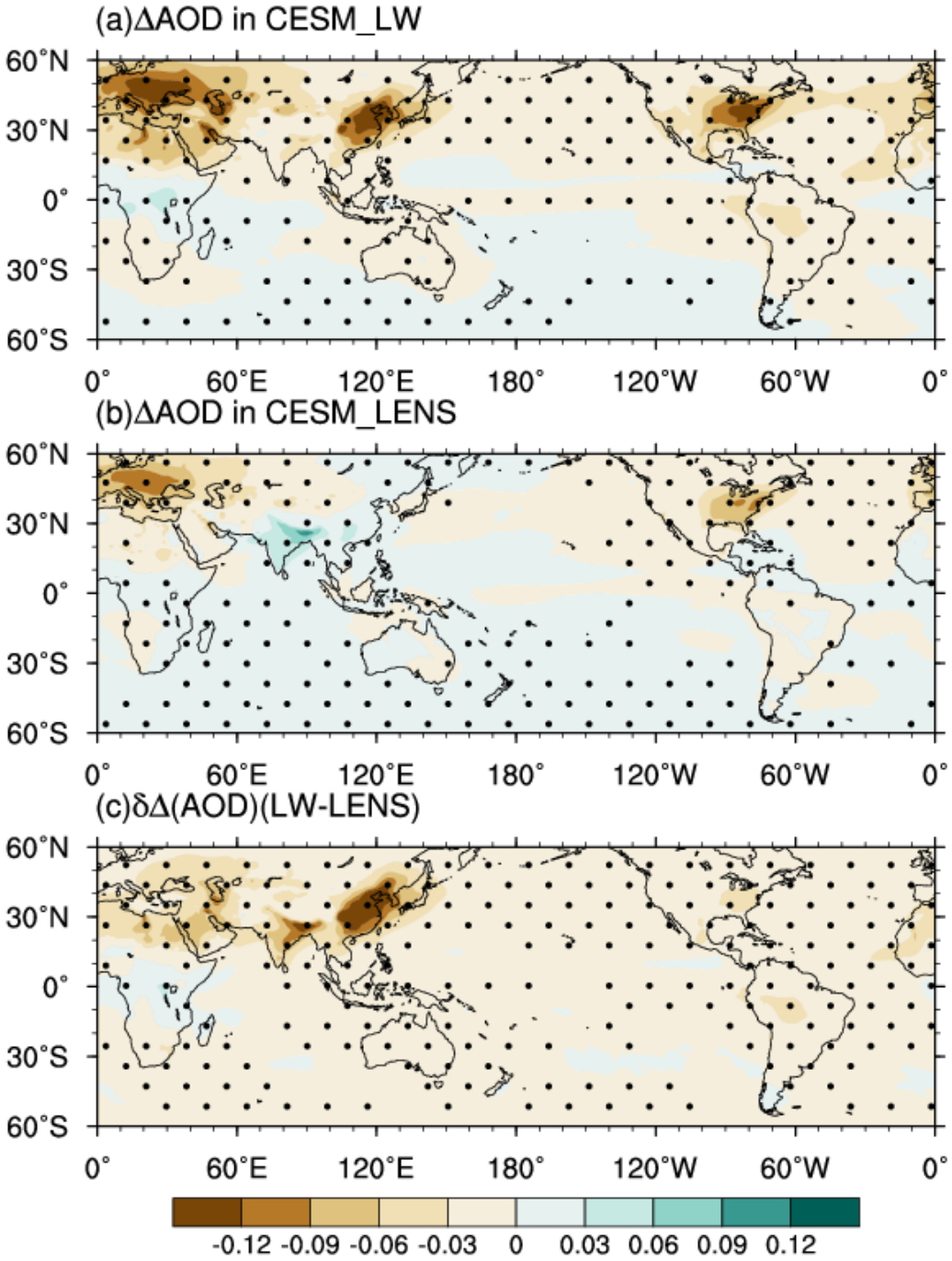

Figure 4. The relative changes of aerosol optical depth (AOD) at 550 nm for the two warming scenarios (future minus present, noted as Δ) and their difference (stabilized minus transient, noted as δ). **a**, ΔAOD under the stabilized warming scenario. **b**, Same as **a** but for the transient warming scenario. **c**, The difference δ(ΔAOD) between the stabilized and transient warming scenarios. Dotted areas in **a** and **b** are statistically significant at the 5% level for the differences between 1.5°C warmer future and present-day, in **c** are statistically significant at the 5% level for the differences between the stabilized and transient scenarios.

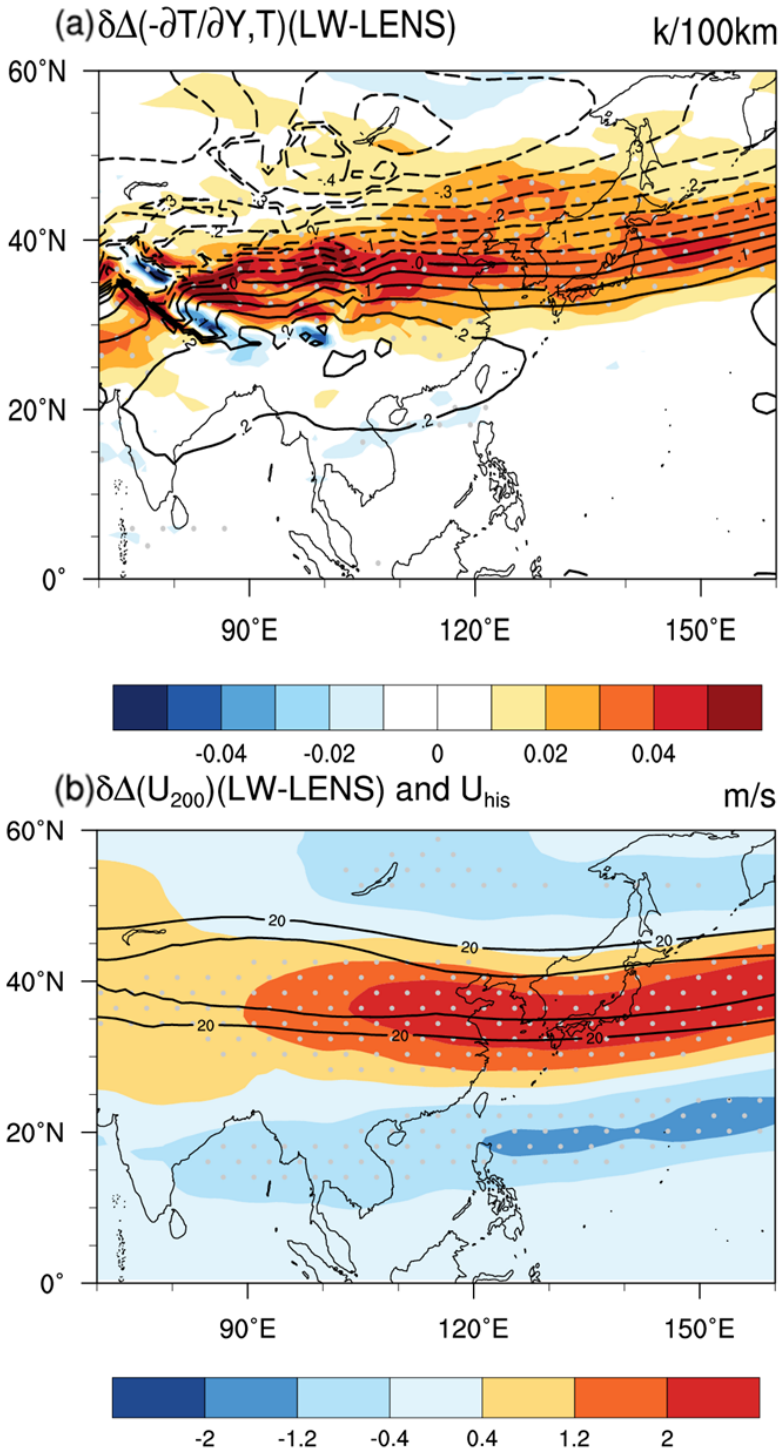

Figure 5. The different responses of the meridional temperature gradient and westly jet in the 1.5°C warmer climate between the stabilized and transient warming scenarios. **a**, The changes in the meridional temperature gradient -∂T/∂Y at 850-200hPa (color shading). The contour lines represent the tropospheric temperature T. **b**, The changes in zonal wind U at 200hPa (color shading). The contour lines represent the historical U. The dotted areas are statistically significant at the 5% level for the differences between the stabilized and transient scenarios.

3.4 Regional atmospheric circulation

The land-ocean thermal contrast and zonal wind changes can explain the changes in regional atmospheric circulation. Actually, the ageostrophic wind equation (see Text S1, Equation S2) provides us an interesting tool of understanding. Figure 6 displays the two inertial-advective components of the ageostrophic wind (horizontal advection of the zonal wind) and their sum. It is clear that the zonal wind gradient shows a significant increase from north of India to southeast China. In the entrance region of the westerly jet, the zonal wind acceleration leads to northward ageostrophic wind at the jet's altitude, as shown in Figure 6c. This excites the secondary circulation with air mass ascending at the south flank of the jet (Diao et al., 2018).

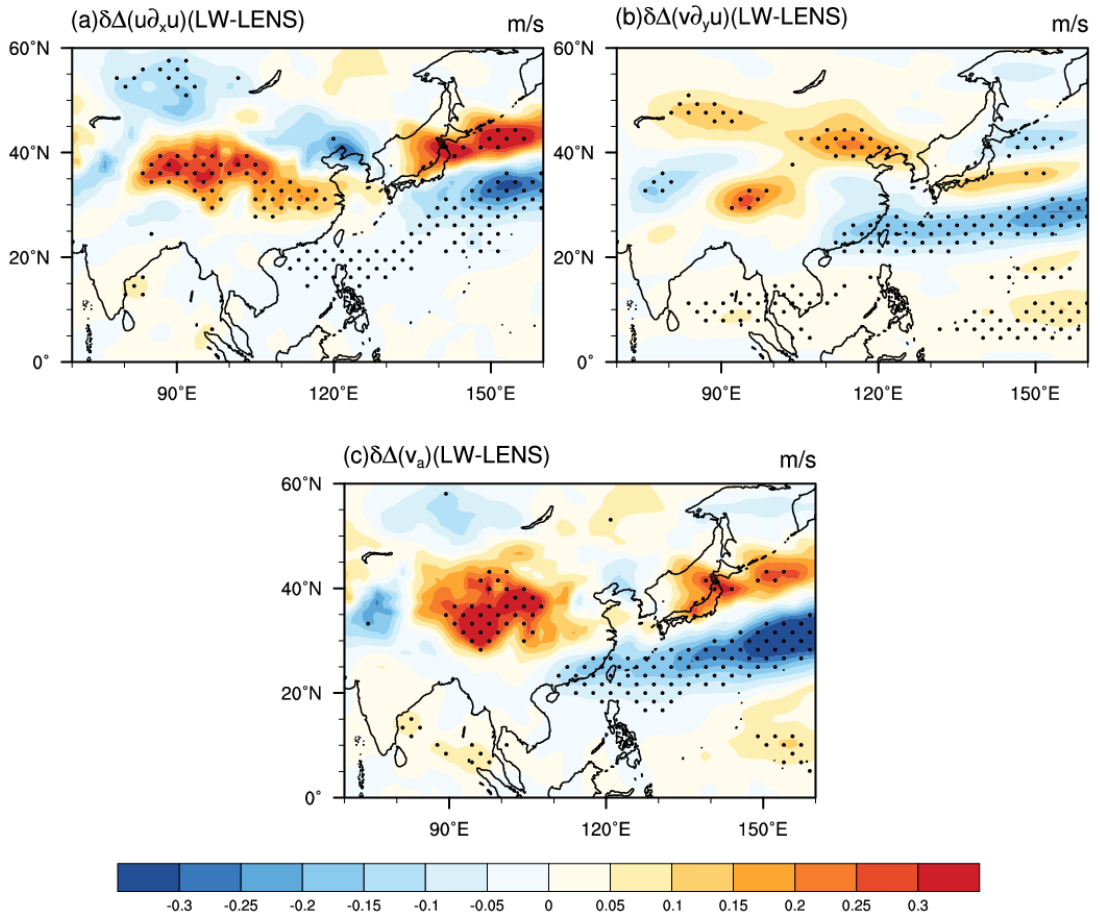

Figure 6. Changes of the ageostrophic wind at 200 hPa (future minus present, and then stabilized minus transient). Panels **a**, and **b** are the two inertial-advective components, u$\partial_x u$. and v$\partial_y u$ while the sum is shown in Panel **c** to represent the ageostrophic meridional wind v_a. Dotted areas are statistically significant at the 5% level for differences between the stabilized and transient scenarios.

Figure 7 then shows a vertical–meridional section of zonal wind changes, as well as the climatological zonal wind averaged over 70°-120°E. For the stabilized warming scenario, the vertical wind shear increases over 30-40°N and the center of the East Asian subtropical westerly jet is also located, with a significant increase (more than 1.6 m/s). A secondary circulation cell due to the ageostrophic wind is clearly present in Figure 7 with ascents near 30°N, and descents beyond 40°N, which is consistent with the northward ageostrophic wind at 200 hPa shown in Figure 6c. It is a direct thermal

cell inducing enhanced precipitation in Southeast China. A few previous studies have already identified a strong relationship between EASJ and summer precipitation in East Asia, that is, EASJ plays an important role in regulating the position of the rain belt in China (Horinouchi et al., 2019). We are thus quite confident that the enhanced meridional temperature gradient and the EASJ lead to larger increased precipitation in southeast China. The large value area of precipitation increase is located near 30°N, on the south side of entrance of the westly jet (Supplementary Figure 3). This explains why the JJA precipitation increases in southeast China in the stabilized warming scenario under the 1.5°C global warming.

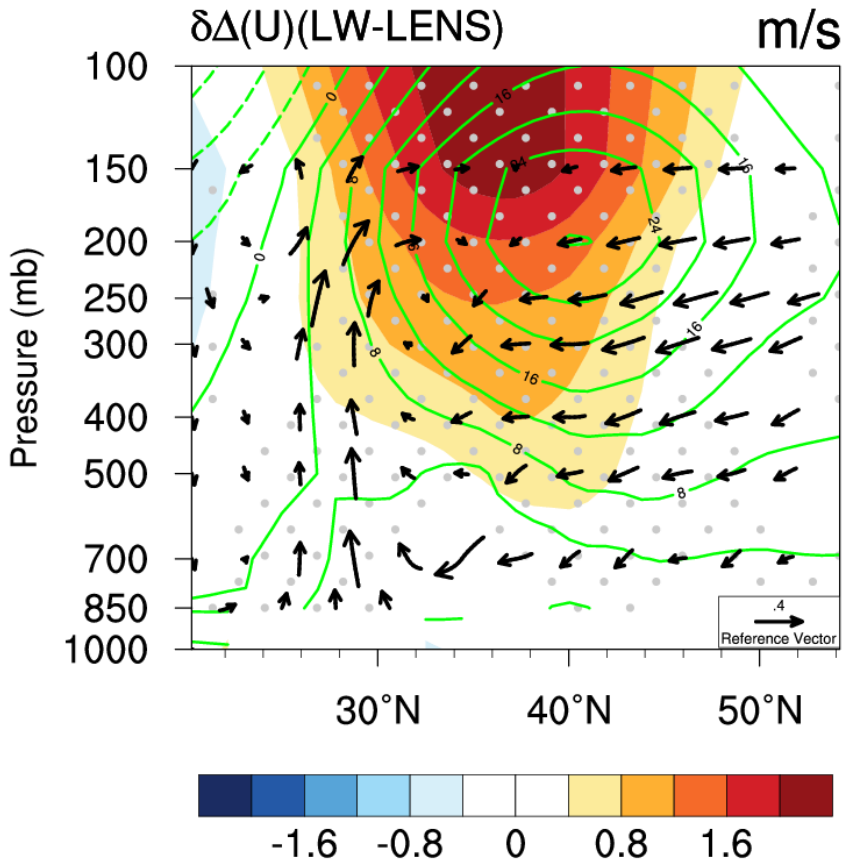

Figure 7. The changes of the atmospheric thermal structure induce a southward shift of the East Asian Westerly Jet and its slight intensification, which creates, perpendicular to the jet, an ageostrophic cell at the entrance zone of the jet. The secondary ageostrophic cell provokes precipitation at its ascending branch in southeast China around 30°N. The vertical–meridional section displays changes (δΔ) of zonal wind U (color shading) and circulation (arrows) averaged over 70°-120°E in the 1.5°C warmer climate (Δ) for the difference (δ) between CESM_LW and CESM_LENS. The green contour lines represent the climatological zonal wind. The dotted areas are statistically significant at the 5% level.

Under the stabilized warming scenario, in parallel to increased precipitation in southeast China, a second zone of increased precipitation, in the form of an arche, is extended from the tropical Indian Ocean off the African coast to the tropical Western Pacific by going through India, Indochina, south of the Philippines, as shown in Figure

9b. This arche zone is the result of enhanced ITCZ and strengthened tropical monsoon. The two clusters of increased precipitation are separated by a decreasing zone in the Western Pacific, extending into the north part of the South China Sea, and even to the north of the Bay of Bengal. But Indochina has more precipitation, playing a role of connection for the two clusters of rainfall in the north and in the south. Figure 8a and 8b shows the changes in the low-level East Asian summer monsoon circulation in the 1.5°C warmer climate, which can easily explain the increase precipitation over India and southeast China. It can be found that the southwest wind at 850hpa from the Indian Ocean to southeast China is stronger under stabilized warming scenario, and there exists a cyclonic circulation over the northwest Pacific, which directly leads to moisture transport and convergence over East Asia. There also exist ascending motions over the tropical Indian Ocean and southeast China, along with the increased water vapor at 850 hPa shown in Figure 8b, which directly leads to increased precipitation over India and southeast China.

We also display in Fig. 8b the changes in MSE (moist static energy, defined as the sum of enthalpy C_PT, geopotential energy gz and latent energy L_vq, symbols being conventional ones) at 850hPa. Previous studies have revealed that areas with strong convection and precipitation nearly coincide with zones of high near-surface moist static energy (Seth et al., 2019). Compared to the transient scenario, the stabilized scenario shows larger MSE at 850hPa close to the equator with maximum values about 0.3×10^3 $(m/s)^2$ over the tropical Indian Ocean. Stronger convective activities and rainfall totals are thus expected to occur in a belt extending from the tropical Indian Ocean to the tropical Western Pacific, with an increase of JJA total precipitation by more than 20mm in most parts of the tropical Indian Ocean.

In response to the additional diabatic heating caused by the enhanced Indian monsoonal precipitation, an atmospheric equatorial Kelvin wave is excited over the Maritime Continent and Western Pacific. This is clearly evidenced by the changes of the regional atmospheric circulation depicted in Figure 9a. In the Indian Ocean region, there is an obvious ascent motion, while the Western Pacific Ocean manifests an obvious descent motion. This Kelvin wave, together with the easterly anomalies created in the western Pacific (Wu et al., 2010) provides the necessary conditions to alter the Western North Pacific (WNP) circulation (Wu et al., 2009). In fact, the easterly wind anomalies of the Kelvin wave decreasing northward off the equator, an anticyclonic atmospheric circulation is created over the Philippine Sea to enhance the Western Pacific Subtropical High in the proximity.

Figure 9b shows the changes of vertically-integrated water vapor flux between the two warming scenarios, as well as the west position of the Western Pacific Subtropical High (WPSH) as defined by He & Zhou, (2015). An anomalous anticyclonic circulation clearly exists in the WNP, which makes intensified westward shifted of the WPSH. This configuration is a very favorable one for a strong northward moisture transport from the South China Sea, and abundant water vapor converges in southeast China, increasing precipitation in this region.

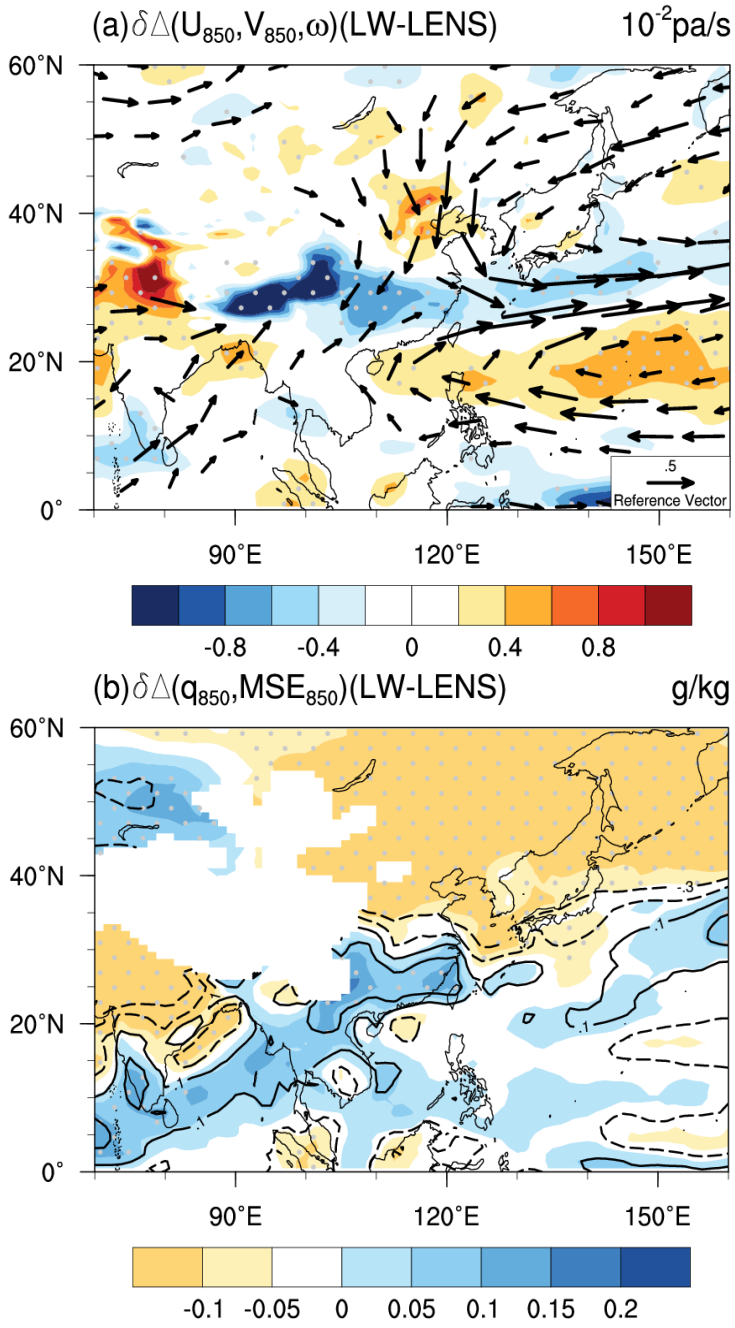

Figure 8. The low-level circulation changes (1.5°C warmer climate minus present-day, then stabilized minus transient) of the East Asian summer monsoon circulation. **a**, Wind vectors at 850hPa and vertical motion at 500hPa. **b**, Specific humidity q (color shaded) and moist static energy (contour lines) at 850hPa. Dotted areas in **a** and **b** are statistically significant at the 5% level for the differences between the stabilized and transient scenarios.

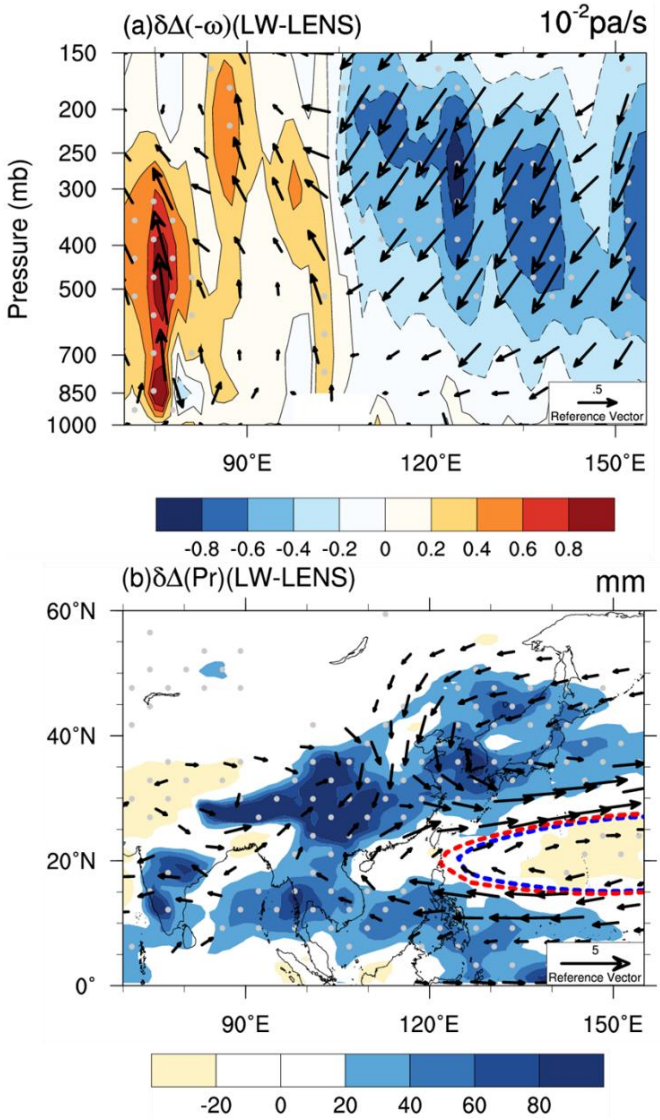

Figure 9. Enhanced precipitation in the tropical Indian Ocean exerts influences on the Western Pacific Subtropical High (WPSH) through a Kelvin wave across the Indo-Pacific region. The WPSH intensified westward shifted increases water vapor transport at its northwest edge and consequently the precipitation belt extending from China to Japan. **a**, Vertical–latitudinal section showing second-order changes (δΔ) of circulation (vectors) and vertical velocity (10^{-2}·pa/s, color shading) averaged over 10°-20°N in the 1.5°C warmer climate (Δ) for the difference (δ) between CESM_LW and CESM_LENS. **b**, The spatial distribution of changes (δΔ) in water-vapor flux integrated from 1000 to 100 hPa (10^{2}·kg·m^{-1}·s^{-1}, vectors) and summer precipitation totals (mm, color shading). The red and blue dotted lines represent the position of the WPSH boundary at 500hPa in CESM_LW and CESM_LENS, respectively. The dotted areas in **a** and **b** are statistically significant at the 5% level for the differences between the stabilized and transient scenarios.

We can now draw a sketch in Figure 10 to summarize the physical processes and mechanisms allowing us to explain the enhanced JJA precipitation in southeast China in the stabilized warming scenario, while the transient warming scenario shows only modest increase of precipitation. The important ingredient is the divergent response of surface warming in the two scenarios. The stabilized scenario shows smaller warming

over land and larger warming over ocean and in the Asian coastal regions (as shown in the upper part of the sketch). Such a land-ocean thermal contrast causes a larger meridional temperature gradient in the atmosphere and enhances the upper-tropospheric westly jet, shifts it southward and creates larger precipitation over southeast China. Furthermore, the ascending motion, accompanying the positive SST and precipitation anomalies over the India Ocean, is able to remotely enhance the anticyclone in the western North Pacific, a favorable situation for abundant moisture circulating from tropical oceans to southeast China.

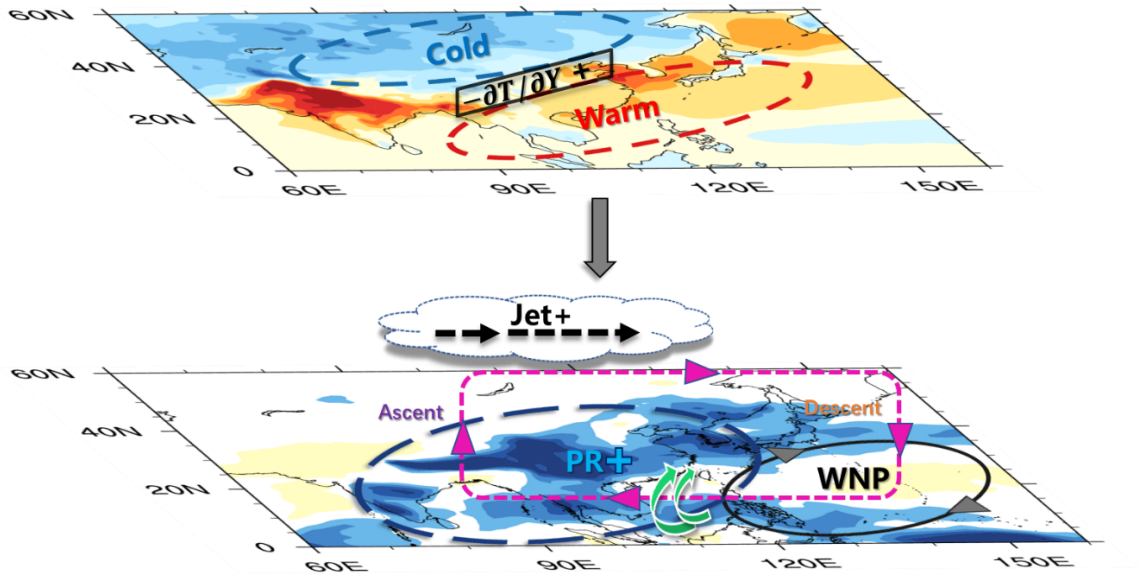

Figure 10. The schematic diagram showing the mechanism for the increase of JJA total precipitation over southeast China in the 1.5°C warmer climate under the stabilized warming scenario compared to the transient scenario. The red (blue) contours indicate positive (negative) surface temperature anomalies. The purple and black dotted arrows represent the enhanced Walker circulation and westly jet, respectively. The green curved arrows represent the moisture transport. The solid circle with arrows represents the anticyclone over the western North Pacific (WNP).

4. Conclusion

The main conclusion drawn from the present study is that two different pathways, leading to the same global warming level of 1.5°C, present however divergent regional responses of JJA precipitation in China. This implies that different adaptation measures should be taken in function of how the warming level is reached while it perfectly respects the Paris Agreement on climate change. The first pathway used in this work is the transient scenario following the RCP8.5 configuration. The second one is the stabilized scenario with global warming maintained at 1.5°C during the simulation.

The regional responses of JJA precipitation were distinctive between the two scenarios. Significant increasing precipitation was shown in southeast China in the stabilized scenario compared with the transient one. The increasing precipitation is 13.3%

larger in the stabilized scenario than that in the transient scenario. By analyzing the water vapor budget equation and decomposing it into dynamic contribution (in relation to changes of atmospheric circulation) and thermodynamic contribution (in relation to changes of water vapor content), it is found that the dynamic effect is the major contributor for the differences between the two pathways to reach the same target of global warming at 1.5°C. The dynamic term is about 0.64 mm/day in southeast China under the stabilized scenario, while only 0.33 mm/day under the transient scenario.

We furthermore analyzed possible mechanisms allowing to explain the difference of precipitation response. It is mainly caused by a differential structure of surface warming which is smaller over land and larger over ocean (as well as along the Asian coasts) in the stabilized scenario. Such a thermal configuration leads to a larger meridional temperature gradient and enhances the East Asia westly jet, causing a direct thermal cell with ascending motion and enhanced precipitation in Southeast China. Simultaneously, stronger convection occurs from the tropical Indian Ocean to the tropical Western Pacific, and leads to a more rigorous India summer monsoon, which is favorable to enhance precipitation and diabatic heating over the tropical Indian Ocean. The equatorial Kelvin wave created and maintained at the east side of the diabatic heating corresponds to easterly wind anomalies over the tropical Western Pacific. The intensity of the Kelvin-wave-associated easterlies decreases away from the equator, which results in an anomalous anticyclone in the western North Pacific. The enhanced westward shifted Western Pacific Subtropical High is then able to transport a larger amount of moisture northward from tropical oceans to southeast China and to enhance the precipitation there.

Finally, we need to point out that the diagnosis and analysis of the present paper are based on simulations of the single model CESM, which may limit the general scope of our conclusions. They need to be further verified with results from multi-models, such as CMIP6 simulations which are progressively available.

Acknowledgments

We acknowledge the CESM team for making their simulations available through the ESGF portals. This work is supported by the National Key Research and Development Program of China (Grant 2017YFA0603804, Grant 2018YFC1507704).

Data Availability Statement

The NCAR CESM historical, RCP and low-warming experiment products were acquired from https://www.earthsystemgrid.org/dataset/ucar.cgd.ccsm4.output.html. The CMIP5 datasets shown in Table S1 are available at https://esgf-node.llnl.gov/projects/cmip5.

References

Alfieri, L., Bisselink, B., Dottori, F., Naumanu, G., Roo, A.d., & P., S. (2016). Global projections of river flood risk in a warmer world. *Earth Future*, *5*(2), 171-182. https://doi.org/10.1002/2016EF000485

Chen, L., Qu, X., Huang, G., & Gong, Y. (2018). Projections of East Asian summer monsoon under 1.5 °C and 2 °C warming goals. *Theoretical and Applied Climatology*, *137*(3-4), 2187-2201. https://doi.org/10.1007/s00704-018-2720-1

Chen, Z., Zhou T., Zhang W., Li P., & Zhao S. (2020). Projected Changes in the Annual Range of Precipitation Under Stabilized 1.5°C and 2.0°C Warming Futures. *Earth Future*, *8*(9), e2019EF001435. https://doi.org/10.1029/2019EF001435

Chevuturi, A., Klingaman, N.P., Turner, A.G., & Hannah, S. (2018). Projected changes in the Asian-Australian monsoon region in 1.5°C and 2.0°C global-warming scenarios. *Earth Future*, *6*(3), 339-358. https://doi.org/10.1002/2017EF000734

Chou, C., Chiang, J.C.H., Lan, C.-W., Chung, C.-H., Liao, Y.-C., & Lee, C.-J. (2013). Increase in the range between wet and dry season precipitation. *Nature Geoscience*, *6*(4), 263-267. https://doi.org/10.1038/ngeo1744

Chou, C., & Lan, C.-W. (2012). Changes in the Annual Range of Precipitation under Global Warming. *Journal of Climate*, *25*(1), 222-235. https://doi.org/10.1175/jcli-d-11-00097.1

Deser, C., R. Knutti., S. Solomon., & A. S. Phillips., (2012). Communication of the role of natural variability in future North American climate. *Nature Climate Change*, *2*(11), 775-779. https://doi.org/10.1038/nclimate1562

Diao, Y., Li T., & Hsu, P.-C. (2018). Influence of the Boreal Summer Intraseasonal Oscillation on Extreme Temperature Events in the Northern Hemisphere. *Journal of Meteorological Research*, *32*(4), 534-547. https://doi.org/10.1007/s13351-018-8031-8

Guan, X., Huang, J., Guo, R., & Lin, P. (2015). The role of dynamically induced variability in the recent warming trend slowdown over the Northern Hemisphere. *Scientific Reports*, *5*, 12669. https://doi.org/10.1038/srep12669

He, C., & Zhou, T. (2015). Responses of the Western North Pacific Subtropical High to Global Warming under RCP4.5 and RCP8.5 Scenarios Projected by 33 CMIP5 Models: The Dominance of Tropical Indian Ocean–Tropical Western Pacific SST Gradient. *Journal of Climate*, *28*, 365-380. https://doi.org/10.1175/JCLI-D-13-00494.1

Horinouchi, T., Matsumura, S., Ose, T., & Takayabu, Y.N. (2019). Jet–Precipitation Relation and Future Change of the Mei-Yu–Baiu Rainband and Subtropical Jet in CMIP5 Coupled GCM Simulations. *Journal of Climate*, *32*, 2247-2259. https://doi.org/10.1175/JCLI-D-18-0426.1

Huang, J., Xie, Y., Guan, X., Li, D., & Ji, F. (2017). The dynamics of the warming hiatus over the Northern Hemisphere. *Climate Dynamics*, *48*, 1-18. https://doi.org/10.1007/s00382-016-3085-8

IPCC Special Report (Cambridge Univ. Press, 2018). *Global Warming of 1.5 °C*.

Kay, J.E., Deser, C., Phillips, A., Mai, A., Hannay, C., Strand, G., et al. (2015). The Community Earth System Model (CESM) Large Ensemble Project: A Community Resource for Studying Climate Change in the Presence of Internal Climate Variability. *Bulletin of the American Meteorological Society*, *96*(8), 1333-1349. https://doi.org/10.1175/bams-d-13-00255.1

King, A.D., Freychet, N., Arblaster, J.M., Lewis, S.C., Mitchell, D.M., Uhe, P., et al. (2018). On the Linearity of Local and Regional Temperature Changes from 1.5°C to 2°C of Global Warming. *Journal of Climate*, *31*(18), 7495-7514. https://doi.org/10.1175/jcli-d-17-0649.1

King, A.D., Lane, T.P., Henley, B.J., & Brown, J.R. (2019). Global and regional impacts differ between transient and equilibrium warmer worlds. *Nature Climate Change*, *10*(1), 42-47. https://doi.org/10.1038/s41558-019-0658-7

Kitoh, A., Endo, H., Kumar, K.K., Cavalcanti, I.F.A., Goswani, P., & Zhou, T. (2013). Monsoons in a changing world: A regional perspective in a global context. *Journal of Geophysical Research: Atmospheres*, *118*(8), 3053-3065. https://doi.org/10.1002/jgrd.50258

Lee, D., Min, S.-K., Fischer, E., Shiogama, H., Bethke, I., Lierhammer, L., et al. (2018). Impacts of half a degree additional warming on the Asian summer monsoon rainfall characteristics. *Environmental Research Letters*, *13*, 044033. https://doi.org/10.1088/1748-9326/aab55d

Li, D., Zhou, T., & Zhang, W. (2019). Extreme precipitation over East Asia under 1.5°C and 2°C global warming targets: A comparison of stabilized and overshoot projections. *Environmental Research Communications*, *1*, 085002. https://doi.org/10.1088/2515-7620/ab3971

Li, H., Chen, H., Wang, H., & Yu, E. (2018). Future precipitation changes over China under 1.5 degrees C and 2.0 degrees C global warming targets by using CORDEX regional climate models. *Science of the Total Environment*, *640-641*, 543-554. https://doi.org/10.1016/j.scitotenv.2018.05.324

Li, W., Jiang, Z.-H., Zhang, X., Li, L., & Sun, Y. (2018). Additional risk in extreme precipitation in China from 1.5°C to 2.0°C global warming levels. *Science Bulletin*, *63*, 228-234. https://doi.org/10.1016/j.scib.2017.12.021

Li, X., Ting, M., Li, C., & Henderson, N. (2015). Mechanisms of Asian summer monsoon changes in response to anthropogenic forcing in CMIP5 models. *Journal of Climate*, *28*(10), 4107-4125. https://doi.org/10.1175/JCLI-D-14-00559.1

Liu, J., Xu, H., & Deng, J. (2018). Projections of East Asian summer monsoon change at global warming of 1.5 and 2 °C. *Earth System Dynamics*, *9*(2), 427-439. https://doi.org/10.5194/esd-9-427-2018

Lo, T.-T., & Hsu, H.-H. (2010). Change in the dominant decadal patterns and the late 1980s abrupt warming in the extratropical Northern Hemisphere. *Atmospheric Science Letters*, *11*(3), 210-215. https://doi.org/10.1002/asl.275

Long, S.-M., Xie, S.-P., Zheng, X.-T., & Liu, Q. (2014). Fast and Slow Responses to Global Warming: Sea Surface Temperature and Precipitation Patterns. *Journal of Climate*, *27*(1), 285-299. https://doi.org/10.1175/jcli-d-13-00297.1

Mueller, B., & S. I. Seneviratne. (2020). Hot days induced by precipitation deficits at the global scale. *Proceedings of the national academy of sciences*, *109*(31), 12398-12403. https://doi.org/ 10.1073/pnas.1204330109

Rogelj, J., Forster, P.M., Kriegler, E., Smith, C.J., & Seferian, R. (2019). Estimating and tracking the remaining carbon budget for stringent climate targets. *Nature*, *571*(7765), 335-342. https://doi.org/10.1038/s41586-019-1368-z

Sanderson, B.M., Xu, Y., Tebaldi, C., Wehner, M., O'Neill, B., & Jahn, A. (2017). Community Climate Simulations to assess avoided impacts in 1.5 °C and 2 °C futures. *Earth System Dynamics*, *8*, 827-847. https://doi.org/10.5194/esd-8-827-2017

Seth, A., Giannini, A., Maisa, R., Rauscher, S.A., Bordoni, S., Singh, D., et al. (2019). Monsoon responses to climate changes—connecting past, present and future. *Current Climate Change Reports*, *5*, 63-79. https://doi.org/10.1007/s40641-019-00125-y

Shi, C., Jiang, Z.-H., Chen, W.-L., & Li, L. (2018). Changes in temperature extremes over China under 1.5 °C and 2 °C global warming targets. *Advances in Climate Change Research*, *9*(2), 120-129. https://doi.org/10.1016/j.accre.2017.11.003

Sun, Y., Zhou, T., Ramstein, G., Contoux, C., & Zhang, Z. (2015). Drivers and mechanisms for enhanced summer monsoon precipitation over East Asia during

the mid-Pliocene in the IPSL-CM5A. *Climate Dynamics*, *46*(5-6), 1437-1457. https://doi.org/10.1007/s00382-015-2656-4

United Nations Framework Convention on Climate Change (UNFCCC, 2015). *Adoption of the Paris Agreement FCCC/CP/2015/L.9/Rev.1* http://unfccc.int/resource/docs/2015/cop21/eng/l09r01.pdf

Wang, B., Wu, R., & Fu, X. (2000). Pacific-East Asian Teleconnection: How Does ENSO Affect East Asian Climate? *Journal of Climate*, *13*, 1517-1536.

Wang, Z., Lin, L., Zhang, X., Zhang, H., Liu, L., & Xu, Y. Y. (2017). Scenario dependence of future changes in climate extremes under 1.5°C and 2°C global warming. *Scientific Reports*, *7*, 46432. https://doi.org/10.1038/srep46432

Wehner, M., Stone, D., Mitchell, D., Shiogama, H., Fischer, E., Graff, L.S., et al. (2017). Changes in extremely hot days under stabilized 1.5 °C and 2.0 °C global warming scenarios as simulated by the HAPPI multi-model ensemble. *Earth System Dynamics*, *9*, 299-311. https://doi.org/10.5194/esd-2017-89

Wei, Y., Yu, H., Huang, J., Zhou, T., Zhang, M., & Ren, Y. (2019). Drylands climate response to transient and stabilized 2 °c and 1.5 °c global warming targets. *Climate Dynamics*, *53*, 2375-2389. https://doi.org/10.1007/s00382-019-04860-8

Wu, B., Li, T., & Zhou, T. (2010). Relative contributions of the Indian Ocean and local SST anomalies to the maintenance of the western North Pacific anomalous anticyclone during the El Niño decaying summer. *Journal of Climate*, *23*, 2974-2986. https://doi.org/10.1175/2010JCLI3300.1

Wu, B., Zhou, T., & Li, T. (2009). Seasonally Evolving Dominant Interannual Variability Modes of East Asian Climate*. *Journal of Climate*, *22*(11), 2992-3005. https://doi.org/10.1175/2008jcli2710.1

Zhai, P., Yu, R., Zhou, B., Chen, Y., Guo, J., & Lu, Y. (2017). Research progress on the global and regional impact of 1.5 °C warming. *Advances in Climate Change Research*, *13*, 465-472. https://doi.org/10.12006/j.issn.1673-1719.2017.159

Zhang, W., & Villarini, G. (2017). Heavy precipitation is highly sensitive to the magnitude of future warming. *Climatic Change*, *145*(1-2), 249-257. https://doi.org/10.1007/s10584-017-2079-9

Zhang, W., & Zhou T. (2020). Increasing impacts from extreme precipitation on population over China with global warming. *Science Bullentin*, *65*(3), 243-252. https://doi.org/10.1016/j.scib.2019.12.002

Zhang, W., & Zhou T. (2021). The Effect of Modeling Strategies on Assessments of Differential Warming Impacts of 0.5°C. *Earth Future*, *9*(4), e2020EF001640. https://doi.org/10.1029/2020EF001640

Zhang, W., Zhou T., Zhang L., & Zou, L. (2019). Future intensification of the water cycle with an enhanced annual cycle over global land monsoon regions. *Journal of Climate*, *32*(17), 5437-5452. https://doi.org/10.1175/jcli-d-18-0628.1

Zhou, T., Zhang, W., Zhang, L., Zhang, X., Qian, Y., Peng, D., et al. (2020). The dynamic and thermodynamic processes dominating the reduction of global land monsoon precipitation driven by anthropogenic aerosols emission. *Science China Earth Sciences*, *63*, 919. https://doi.org/10.1007/s11430-019-9613-9

Supporting Information for

Divergent Responses of Summer Precipitation in China to 1.5°C Global Warming in Transient and Stabilized Scenarios

Zhihong Jiang[1,2]*, Qiyao Hou[1], Tim Li[2,3], Yongxiao Liang[1,4], Laurent Li[5]

[1]*Joint International Research Laboratory of Climate and Environment Change, Collaborative Innovation Center on Forecast and Evaluation of Meteorological Disaster, Nanjing University of Information Science and Technology, Nanjing* 210044, *China*.

[2]*Key Laboratory of Meteorological Disaster of Ministry of Education, Collaborative Innovation Center on Forecast and Evaluation of Meteorological Disaster, Nanjing University of Information Science and Technology, Nanjing* 210044, *China*.

[3]*International Pacific Research Center (IPRC), and Department of Atmospheric Sciences, SOEST, University of Hawaii at Manoa, Honolulu, HI 96822, USA.*

[4]*School of Earth and Ocean Sciences, University of Victoria, Victoria, British Columbia, Canada.*

[5]*Laboratoire de Météorologie Dynamique, IPSL, CNRS, Sorbonne Université, Ecole Normale Supérieure, Ecole Polytechnique, Paris* 75005, *France*.

Corresponding author: Zhihong Jiang (zhjiang@nuist.edu.cn)

Contents of this file

Text S1. Ageostrophic wind at entrance zone of a jet stream

Associated to zonal wind acceleration (or deceleration) at the entrance (exit) zone of a jet stream, a secondary circulation perpendicular to the main zonal wind is excited and can be described by the ageostrophic wind equation:

$$v_a = \frac{1}{f}\frac{du}{dt} \quad (1)$$

where v_a is the meridional ageostrophic wind, $\frac{du}{dt}$ the zonal wind acceleration, expressed as a total (Lagrangian) derivative of the zonal wind, and f the Coriolis parameter. Eq. 1 can be further transformed into its Eulerian form (local tendency and advective components):

$$v_a = \frac{1}{f}(\partial_t u + u\partial_x u + v\partial_y u) \quad (2)$$

$\partial_t u$ in Equation 2 is the time partial derivative of u, which can be ignored since its long-term mean is much smaller than other terms. The zonal wind gradient in zonal direction plays a leading role in the change of jet-induced ageostrophic wind. In the Northern Hemisphere, the entrance zone of a jet stream produces a northward ageostrophic wind, creating a direct thermal circulation with ascent in the south and descent in the north. The Eulerian form of the ageostrophic wind equation is particularly helpful for us to calculate the ageostrophic wind and to interpret changes of atmospheric circulation due to global warming or between the stabilized and transient scenarios.

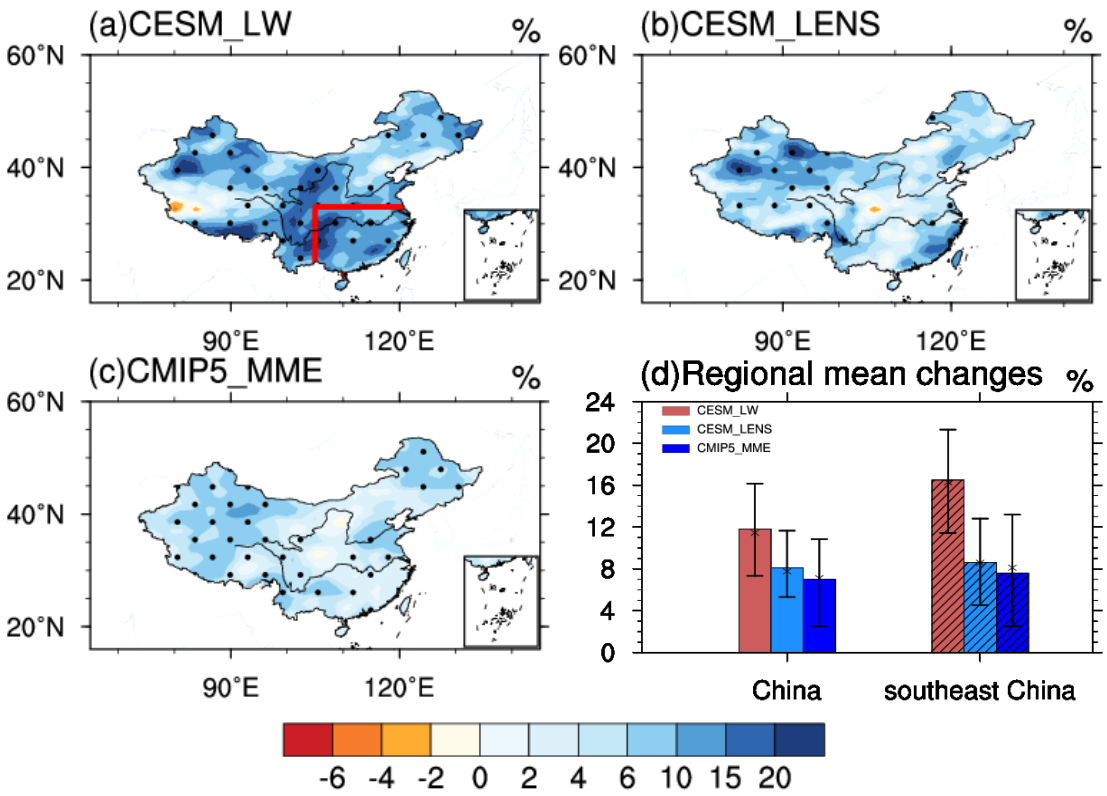

Figure S1. Same as Figure 1, but for the relative changes in JJA Rx5day (relative to 1986-2005, considered as present-day climate) in the 1.5°C warmer climate (relative to preindustrial).

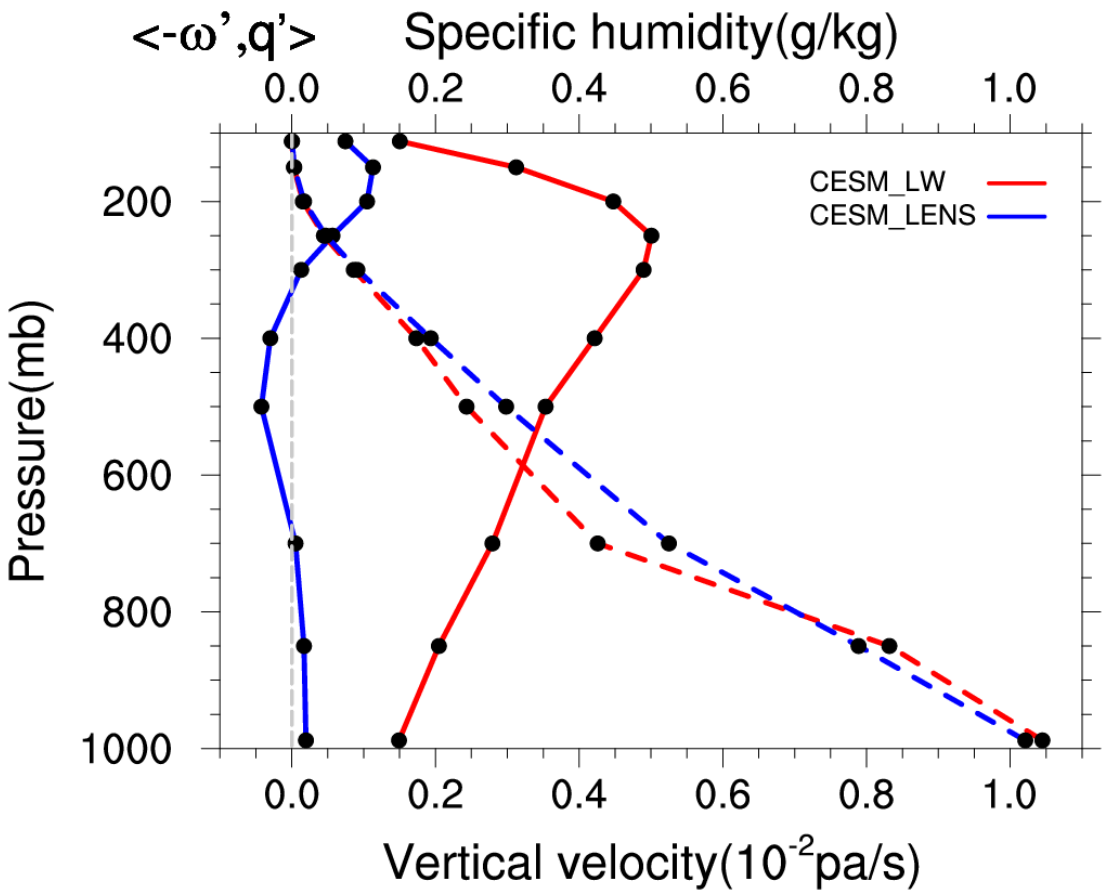

Figure S2. The vertical profiles of the changes in vertical velocity ω (solid line with circle markers, 10^{-2}pa/s) and specific humidity q (dash line with triangle markers, g/kg) averaged over southeast China (22-33°N, 105-122°E, land areas) in the 1.5°C warmer climate. The red and blue lines represent the results in CESM_LW and CESM_LENS, respectively.

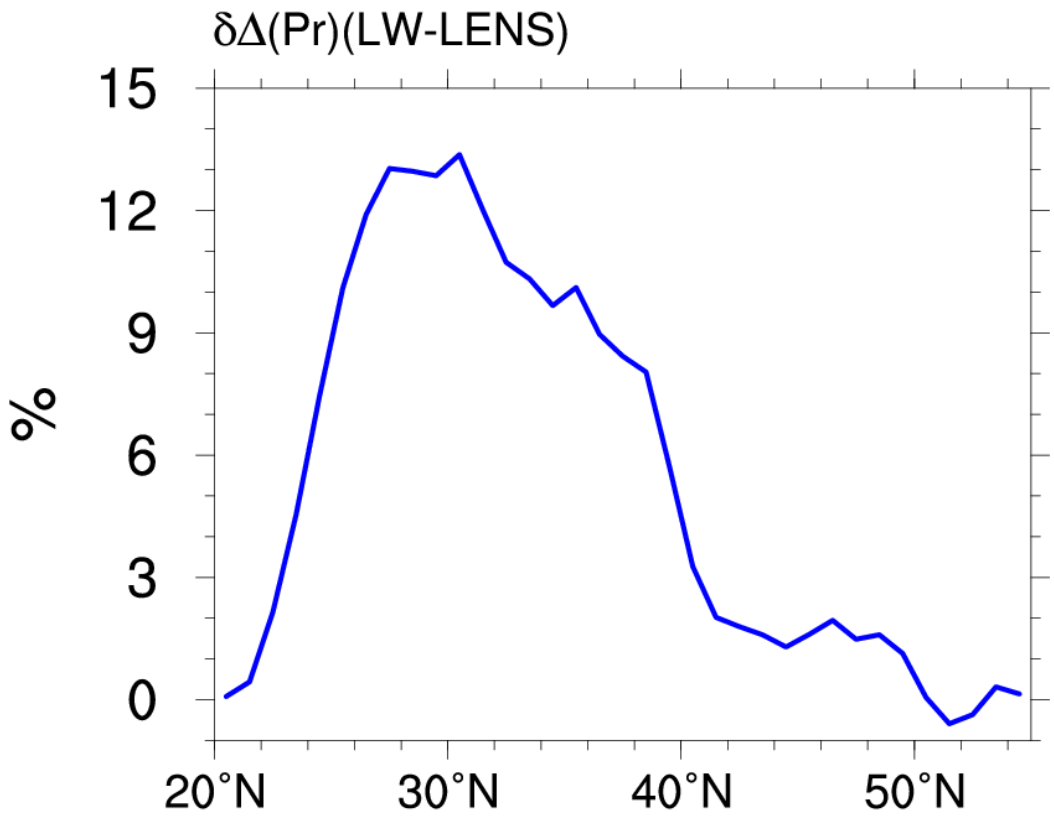

Figure S3. The enhanced precipitation in Southeast China resulted from a direct thermal cell with ascending motion. The meridional profile of changes in precipitation averaged over 105°-122°E in the 1.5°C warmer climate for the difference between CESM_LW and CESM_LENS.

Table S1. Names, atmospheric horizontal resolutions and model centers of the 21 selected CMIP5 models.

Model name	**Atmospheric resolution (lat × lon)**	**Modeling center and country**
BCC-CSM1-1	2.81258°× 2.81258°	Beijing Climate Center, China Meteorological Administration, China
BCC-CSM1-1-M	1.125°×1.12°	
BNU-ESM	2.8°×2.8°	
CanESM2	2.8°×2.8°	Canadian Centre for Climate Modelling and Analysis, Canada
CCSM4	1.25°×0.94°	National Center for Atmospheric Research, United States
CNRM-CM5	1.4°×1.4°	Centre National de Recherches Météorologiques– Centre Européen de Recherche et de Formation Avancée en Calcul Scientifique, France
CSIRO-Mk3-6-0	1.875°×1.875°	Commonwealth Scientific and Industrial Research Organization, Australia
FGOALS-g2	2.8°×1.4°	Flexible Global Ocean-Atmospheric-Land System Model gridpoint
GFDL-CM3 GFDL-ESM2G GFDL-ESM2M	2.5°×2.0°	NOAA/Geophysical Fluid Dynamics Laboratory, United States
HadGEM2-ES	1.875°×1.24°	The Met Office Hadley Centre, United Kindom
IPSL-CM5A-LR	3.75°×1.895°	L'Institut Pierre-Simon Laplace, France
IPSL-CM5A-MR	2.5°×1.27°	
MIROC5	1.40625°×1.40625°	National Institute for Environmental Studies, The University of Tokyo, Japan
MIROC-ESM	2.815°×2.815°	
MIROC-ESM-CHEM	2.815°×2.815°	
MPI-ESM-LR	1.875°×1.875°	Max Planck Institute for Meteorology, Germany
MPI-ESM-MR	1.875°×1.875°	
MRI-CGCM3	1.125°×1.125°	
NorESM1-M	1.8725°×2.5°	Norwegian Climate Centre, Norway

Table S2. The regional average of JJA precipitation in China and southeast China for three sets of ensemble simulations. the number in brackets represent the minimum and the maximum of the ensemble members. σ is the standard deviation of the ensemble members. Units: %.

	China	southeast China
CESM-LW	**12.1**(9.9-17.0), σ=2.2	**19.3**(12.5-21.8), σ=2.8
CESM-LENS	**7.4**(4.4-10.2), σ=2.0	**6.0**(2.3-9.0), σ=2.4
CMIP5-MME	**5.2**(1.2-9.8), σ=2.5	**3.7**(-3.1-8.8), σ=3.0